Composite Structures 341 (2024) 118216

Contents lists available at ScienceDirect

Composite Structures

journal homepage: www.elsevier.com/locate/compstruct

The influence of R/t-ratio on the imperfection sensitivity of the buckling load of thin-walled CFRP cylindrical shells

Tobias S. Hartwich [a,*], Stefan Panek [a], Dirk Wilckens [b,c], Tobias Wille [b], Dieter Krause [a]

[a] TUHH, Institute of Product Development and Mechanical Engineering Design, Denickestraße 17, 21073 Hamburg, Germany
[b] DLR, Institute of Lightweight Systems, Lilienthalplatz 7, 38108 Braunschweig, Germany
[c] now: ArianeGroup, Bremen, Germany

ARTICLE INFO

Keywords:
Buckling
Composite shells
Imperfections
Test rig

ABSTRACT

Thin-walled cylindrical shells under axial compression load are prone to buckling. The influencing factors leading to a reduction of the buckling load are a major design challenge. The sensitivity to imperfection increases with rising slenderness. In literature, cylinders with the same parameters and different slenderness are rarely tested in a larger number of samples. In this contribution, seven cylindrical shells, six of them nominally identical, are tested on two different test rigs and compared with twelve specimens with a smaller radius and same wall thickness from a previous series of tests. It is shown how the imperfection sensitivity is dependent on the R/t-ratio. Additionally, it is demonstrated how the quality of the test set ups corresponds with the achieved buckling load. Finally, the suitability of selected design approaches is determined based on the test results. Based on that, recommendations for the choice of a suitable approach are given.

1. Introduction

Thin-walled cylindrical shells are widely utilised structures in aerospace engineering [1,2]. Due to the field of application there are high demands on lightweight design, reliability and cost [1]. Under compressive load, thin-walled structures are prone to buckling [3]. Thus, buckling drives the design of thin-walled shell structures of launch vehicles [2]. A major challenge is the existing discrepancy between theoretical and experimental buckling load due to imperfections [3]. As the investigation of the buckling behaviour of thin-walled cylindrical shells has been subject of research for many decades, the factors which influence the buckling load are sufficiently well known [4]. Especially for isotropic shells, there is extensive research on the matter of accounting for geometric imperfections starting already in the early 20th century, like [5]. Nevertheless, especially in case of cylinders made from fibre-reinforced plastic composites, either tests are necessary to quantify the different influencing factors due to their large number, or very conservative assumptions are accepted mostly based on metallic cylinders, as is the case in NASA SP-8007, even in the second revision [4]. In order to take these influencing factors into account, there are several approaches to design thin-walled shells. The most common design approach is given in the NASA SP-8007 [4]. This guideline suggests a global knockdown factor considering all imperfections and uncertainties depending on the R/t-ratio. Nevertheless, it often results in very conservative designs [6,7]. One well discussed approach is the Single Perturbation Load Approach (SPLA) postulated by Hühne, which only needs nominal data and yields less conservative design loads than the NASA SP-8007 [8]. However, in some cases these design loads are not conservative [9–12]. Since most imperfections are of stochastic nature, probabilistic approaches appear promising, like [11,13–15]. Besides high computational cost, the main drawback of probabilistic approaches is that distributions of all relevant influencing parameters have to be available or need to be assumed.

A good summary of tested cylindrical CFRP shells can be found in [16–18] or [19]. Most available tests are limited to small sample sizes and rather low R/t-ratios, as shown for instance in [19,20]. In most cases, the cylinders in individual publications have three to ten layers and the same nominal radius [19]. Often there is one fixed or most commonly used radius per research group [20]. However, it is well known that the R/t-ratio is a key factor for imperfection sensitivity. Nevertheless, few cylinders have been investigated so far that have varying R/t-ratios with otherwise identical parameters. This is mostly realised by keeping the radius constant and doubling the number of layers, i.e. in [21–23]. In [24], however, the layer structure is kept unchanged and the radius is varied. In total, a variation of the R/t-ratio while keeping other parameters constant is addressed in 49 of the 218 experiments available in [19]. Furthermore, as shown in [25], the test rig influence is rarely investigated. In [25–28] test rig comparisons are conducted and it is shown that the test rig influence may be of the same

* Corresponding author.
E-mail address: tobias.hartwich@tuhh.de (T.S. Hartwich).

https://doi.org/10.1016/j.compstruct.2024.118216
Received 8 March 2024; Received in revised form 2 May 2024; Accepted 15 May 2024
Available online 18 May 2024

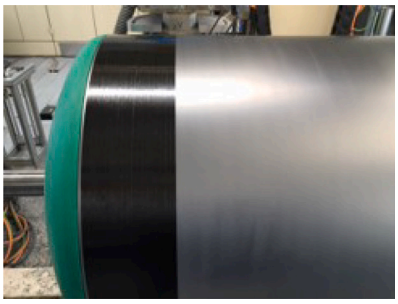

Fig. 1. Winding mandrel.

magnitude as other factors like geometric imperfections. By comparing results from different test rigs, it is possible to classify the quality of test data, which is essential for validation of design approaches.

In general, new approaches are often validated against these available data [1]. Many of the data sets are very similar, as frequently not all information is freely available and the number of test specimens is comparatively small [20]. If indicated in the respective publications, most of the shells are produced either by manual hand lay-up or filament winding processes [19]. Comparisons to quantify the manufacturing process' influence are rarely conducted in the existing database. In [29], for example, it is shown that the crossovers occurring during filament winding can cause local buckling. In [25], six shells manufactured in hand layup and filament winding are compared with each other. It can be shown that the amplitudes of geometric imperfections are comparable while imperfection patterns resulting from filament winding are significantly more regular [25]. The samples produced by filament winding achieved comparable buckling loads [25].

The purpose of this paper is to investigate the effects of the R/t-ratio on the imperfection sensitivity of the buckling load by changing the manufacturing process and the test rig. For this objective, seven thin-walled cylindrical shells with a nominal R/t-ratio of 375 are tested on two different test rigs. Afterwards, the results are compared with those of 12 cylinders with an R/t-ratio of 142 under otherwise identical manufacturing and test conditions. In order to provide data which are suitable for validation of design approaches, the quality of the test data is analysed. Since imperfection sensitivity must be taken into account in the determination of design loads, it is examined whether common design approaches such as NASA SP-8007, the SPLA, frequentist Monte Carlo Analyses or a linear buckling mode shape imperfection (LBMI) include the experimentally determined imperfection sensitivities. Since possible uneven conditions in the load introduction reduce the buckling load, the Single Boundary Perturbation Load Approach (SBPA), as postulated in [30], is also analysed regarding its suitability.

Finally, this paper adds more cylinders to the available database. With these data, other researchers can validate their design approaches.

2. Manufacturing process and test setup

2.1. Manufacturing process and specimen preparation

The seven cylindrical shells investigated in this contribution were manufactured at German Aerospace Center (DLR) in Braunschweig. Six of these were manufactured in a semi-automatic hand lay-up process and one by filament-winding. As the cylinders are comparatively large, one shell was produced per batch. The left half of the winding mandrel is depicted in Fig. 1.

In order to achieve good comparability with the cylinders from [25], AS7/8552 was chosen as the fibre matrix system as well as the same lay-up. As in [25] a 1/4″ slittape is used and the curing is also done in an autoclave. Again, in the hand-laminating process, two 30° layers cannot be laid on top of each other without lifting the lower one again when depositing. Hence these cylinders only have a balanced laminate. The exact distribution of the 30° layers of the wound cylinder results from the winding process. Therefore, the nominal lay-up is given here. For all shells, the lamina angle of the inner and outermost layer is 90.19°. In summary, the same manufacturing parameters as in [25] were chosen for maximum comparability.

Table 1
Geometric specification of the cylinders.

	Z1LG - Z6LG	Z1WG
Nominal inside radius [mm]	300	300
Total length [mm]	800	800
Free length [mm]	750	750
Nominal R/t-Ratio	375	375
Fibre/Matrix	$AS7/8552$	$AS7/8552$
Laminate Layup	$[90°, -30°, 30°, -30°, 30°, 90°]$	$[90°, -30°, 30°]s$
Fabrication Process	$laid\ layer\ by\ layer$	$filament-winding$

All shells have a nominal inside radius of 300 mm, resulting in an R/t-ratio of 375 with a nominal wall thickness of 0.8 mm. Thus, the cylinders are comparatively thin-walled and there is considerably less data in this range, as shown for instance in [20]. All specifications of the seven cylinders are summarised in Table 1. In order to realise a connection from the shell to the test rig, the cylinders are fixed in a clamping specially designed for these shells which is based on the concept of [7]. Fig. 2 shows the cross-section of a clamped cylinder. The shell is clamped at the top and bottom via the inner ring. There is no contact with the outer ring. The space between both rings and the shell is filled with a resin and quartz powder mixture. The outer rings have a wave pattern on the inside so that torque can also be applied in later tests. In contrast to the clamping from [7], the present clamping was made of aluminium and designed as circular rings, so that the mass is easier to handle in the experimental setup. The necessary rigidity of the test set-up is achieved in experiments using the Hexapod via the upper and lower adapter plates, which are made of steel. The cylinder and adapter plates are centred to each other using centring elements. The lower adapter plate is centred on the load cell via a fitting hole and a centring cylinder.

After fabrication and clamping in the test fixtures, all cylinders were measured with an ATOS system in order to quantify geometric imperfections. These are analysed afterwards in terms of patterns resulting from the lay-up and manufacturing process. Due to the ring-shaped structure of the fixtures, the clamped shells can be measured from the outside as well as inside. Based on these measurements, the wall thickness of all shells can be determined. Fourier coefficients for approximating the cylinder surface are calculated from the measurement data for later consideration of geometric imperfections in FE calculations. A double Fourier series with full waves in circumferential direction and cosine half waves in axial direction is utilised. The imperfection measurements of the outside of the cylinders are used in this step so that effects from the laminate structure as well as fibre overlap are included.

2.2. Test setup

Two different test rigs are utilised to quantify the influence of the test rig. On one hand, the Hexapod test rig at the TUHH is used, on the other hand the buckling facility of the DLR in Braunschweig. The Hexapod at TUHH consists of a movable platform that is actuated via six hydraulic cylinders. Uniaxial and multiaxial static and dynamic tests are possible with this test rig [31]. In the scenario focussed here, the test specimen is located underneath the platform, mounted on a 6 DoF load cell. Fig. 3 shows the test setup. By lowering the platform, axial load is applied to the cylinder [32]. The shells are fitted in the clamping presented in Section 2.1. The aforementioned adapter plates are also used in this test setup. The connection to the Hexapod platform is realised via an adapter, which was already used during the tests in [25].

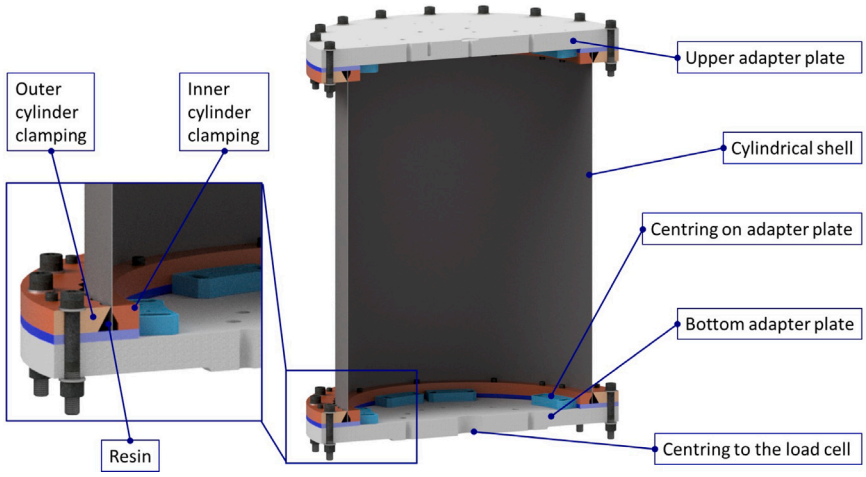

Fig. 2. Clamping of the cylindrical shell.

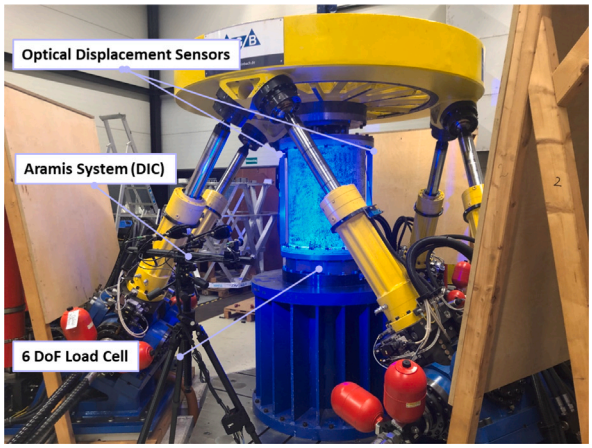

Fig. 3. Test setup of the Hexapod at the TUHH with Z6LG.

The connection is realised by screws, with the platform aligned in such a way that after tightening the screws, the connection is force-free.

In addition to axial compression load, all lateral reaction forces and moments are measured via the 6 DoF load cell underneath the cylinder. The compression of the shell itself can be measured and the tilting calculated via three laser displacement sensors arranged around the circumference. Furthermore, six axially aligned strain gauges are placed circumferentially to measure local strains. In case of shell Z6LG, only three strain gauges are used. Instead of the remaining ones, the strain is measured from one side with an ARAMIS measuring system using Digital Image Correlation, as has been common practice in recent experimental campaigns, e.g. [33,34].

Secondly, the CFRP cylinders were tested under axial compression in the buckling test facility at the Institute of Composite Structures and Adaptive Systems of DLR (Fig. 4). The tested shell is located between the load distributor that is connected to an axially supporting top plate with three load cells, and a lower drive plate. The top plate can be moved in vertical direction on three spindle columns to adapt the test device to the actual test article length. A thin epoxy concrete layer consisting of epoxy reinforced with a mixture of sand and quartz powder is applied between both end plates of the test specimens and the adjacent parts of the test device, i.e. the drive plate and the load distributor. This procedure is done to ensure a uniform load introduction on the shells during loading.

Table 2
Test design of the buckling tests, order of the used test rigs for each cylinder.

	Z1LG	Z2LG	Z3LG	Z4LG	Z5LG	Z6LG	Z1WG
Hexapod fixed	x	x	x	x	x		x
DLR buckling test facility					x	x	
Hexapod fixed						x	

Loads and axial displacements are recorded during the tests. The actual reaction forces are measured by three load cells (100 kN each). The axial displacement is extracted by three displacement transducers, fixed between load distributor and axial drive plate and placed around the test specimen at 90°, 180° and 270°. The shortening used for the load-shortening curves is the average value of the displacement transducers. Strain gauges and optical buckling pattern measurements were not used in this study since the only purpose is the comparison of the buckling load. Axial compression is applied displacement controlled. Before initial buckling occurs, the load is applied stepwise until buckling and unloaded after 5 s in the early post buckling regime to avoid damaging the structure.

In order to allow for identification of possible test rig influences, the following test plan is determined. First, the cylinders Z1LG to Z5LG and Z1WG are tested on the Hexapod. Initially, six compression and tensile tests are carried out in the elastic range. Then, load is applied in a displacement controlled manner at a speed of 0.045 mm/s until buckling occurs. Upon buckling, the displacement is immediately stopped and the cylinder is unloaded, as the post-buckling regime is of no further interest to this study. This is repeated at least ten times for the purpose of providing statistical evidence. The cylinder Z5LG is then tested on the buckling facility of the DLR institute in Braunschweig. The shell Z6LG is first tested on the buckling facility in Braunschweig and afterwards on the Hexapod. Table 2 illustrates the test sequence on the individual test rigs.

2.3. Numerical analysis

Following the experiments, numerical investigations are carried out to analyse the sensitivity of the considered shells regarding different influencing factors. The utilised model and procedure here are based on the one already used in [25]. Commonly, a free length model is utilised which only includes the free shell length between the clampings. In addition, a full length model is set up, considering the total length of the shell including the parts encased in epoxy within the clamping. FE-simulations are run in Abaqus/Standard. For calculations regarding

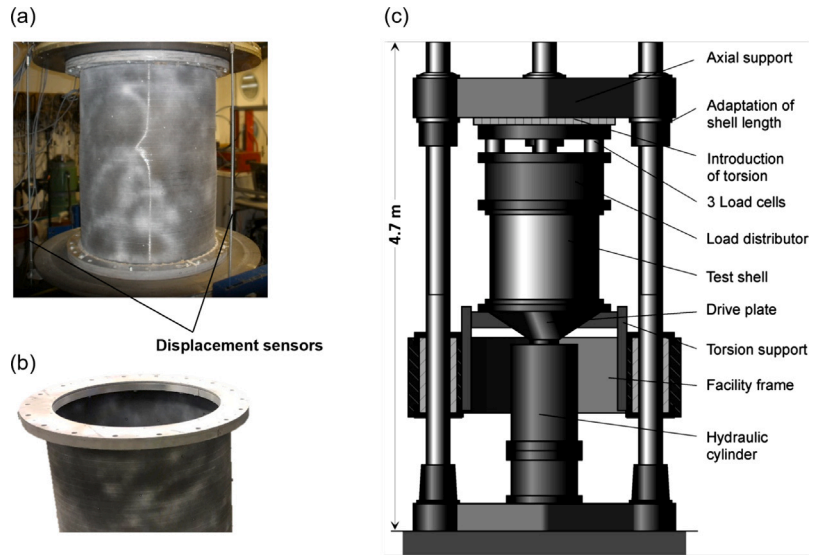

Fig. 4. Test setup of the DLR buckling facility: (a) tested shell in the test rig, (b) clamped cylindrical shell as tested, (c) test rig.

perfect shells, Eigenvalue analyses are used, whereas to find the buckling loads of imperfect shell models, nonlinear analyses with artificial damping and load control are applied. The cylinders are modelled using S4R shell elements with a characteristic length of 3 mm, resulting in a mesh of 250 × 629 elements for the free length or 267 × 629 for the total length of the shells. This mesh size is chosen as it delivers the best ratio of accuracy to computing time. In comparison, a characteristic element length of 1 mm yields only a 1% decrease in buckling load relative to the chosen mesh.

Geometric imperfection patterns are applied to the model using Fourier decomposition of the previously measured real shell geometry. As the shells investigated in this study are manufactured from the same fibre/matrix composite as those in [25], material parameters for FE-modelling are also calculated based on the coupon tests from [35] using the measured wall thicknesses. CFRP exhibit different stiffness properties under tensile and compressive load, as has been previously shown, e.g. in [6]. Thus, a generalised bimodular material model is implemented. Based on stress analyses, tensile stiffness values are applied to the 90° layers, while for the ±30° layers the longitudinal Young's modulus is scaled by 0.91 which gives a good approximation of the corresponding compressive stiffness [25].

The implemented boundary conditions ensure a fully clamped state at the bottom shell edge, whereas the top edge is rigidly tied to a master node that remains unconstrained in lateral direction, which allows for including load imperfections. In order to account for the influence of the clamping, additionally an advanced model is set up that includes the epoxy resin and contact interactions to the shell as well as to the inner and outer ring of the clamping at both shell edges, similar to the model detailed in [11]. Herein, the aluminium rings are modelled using rigid shell elements. This simplification is considered acceptable, as the stiffness of those rings is expected to be far greater than that of the epoxy. In case of the advanced model, boundary conditions are applied to the rigid clamping instead of the shell itself.

Firstly, the influence of geometric imperfections is analysed by applying the different measured imperfection patterns to a standardised model with a layer thickness of 0.133 mm and appropriately scaled material parameters. Following that, effects and interactions between different recorded types of imperfection are investigated through stepwise superimposition of different factors in nonlinear simulations for each tested shell. The additional imperfections correspond to the influencing factors measured during experiments, including lateral forces, torsional moments, and tilting of the upper shell edge. A comparison of the results to the perfect buckling loads may then allow for ascertaining the magnitude of different influences.

Finally, a selection of established design approaches is applied to the considered shells and compared with regards to reliability and precision of resulting design loads. Using nominal data, deterministic approaches according to NASA SP-8007, SPLA, SBPA and the LBMI are carried out. Regarding the LBMI it was shown in [36] that increasing imperfection amplitudes to greater than the wall thickness results in a plateau of the buckling load, similar to the behaviour observed in the SPLA. Hence, amplitudes are chosen accordingly. Furthermore, it has been shown, e.g. in [37], that a lower bound of the buckling load may in some cases be found when considering buckling modes corresponding to larger eigenvalues or by combination of different eigenmodes. By reason of practicability however, as demonstrated in [37], in this study only the first eigenmode corresponding to the first eigenvalue is chosen as imperfection pattern. In addition, probabilistic design procedures are applied by way of a Frequentist Monte-Carlo (FMC) analysis and the Semi-Analytical Probabilistic procedure (SAP) introduced in [14]. Furthermore, the Probabilistic Perturbation Load Approach (PPLA), detailed in [15], is utilised, thus including a semi-probabilistic approach as well.

3. Test results

3.1. Geometric imperfections

The geometry of all investigated shells was measured both, inside and outside using a photogrammetric measurement system, allowing to calculate the average radius and wall thickness as well as the scatter of both parameters. Furthermore, Fourier coefficients of the geometric imperfections are calculated and published in an open access repository at the TUHH in [38]. The measurement data from the inside surfaces yield an average inside radius of 300.2 mm for all shells which is slightly larger than the nominal one. The outside radius averages 301.05 mm. The outside radii as well as the imperfection range, wall thickness and resulting R/t-ratio are presented in Table 3 for each shell. The spread of geometric imperfections of each individual shell is shown in Fig. 5 in separate histograms. The cylinder Z1LG has the largest imperfection range. Z4LG, Z3LG and Z2LG show the smallest one, whereas Z5LG and Z6LG possess similar imperfection range and spread. The wound cylinder Z1WG falls into the middle of the range of geometric imperfections of all shells.

While all shells exhibit a prominent ovalisation mode, as visualised in Fig. 6, the filament-wound shell Z1WG shows a notably more regular pattern compared to the layered ones. In addition, the crossing sections

Table 3
Measured geometric specification of the cylinders.

	Z1LG	Z2LG	Z3LG	Z4LG	Z5LG	Z6LG	Z1WG
Radius [mm]	301.0 ± 0.3	301.0 ± 0.1	301.1 ± 0.1	301.1 ± 0.1	301, 0 ± 0.1	301.1 ± 0.1	301.1 ± 0.1
Imperfection range [mm]	[−0.74, 0.69]	[−0.40, 0.32]	[−0.18, 0.39]	[−0.18, 0.29]	[−0.45, 0.63]	[−0.36, 0.66]	[−0.27, 0.37]
Wall thickness [mm]	0.80 ± 0.04	0.86 ± 0.03	0.87 ± 0.04	0.84 ± 0.04	0.84 ± 0.03	0.85 ± 0.03	0.88 ± 0.04
R/t-Ratio	376	350	354	358	358	354	342

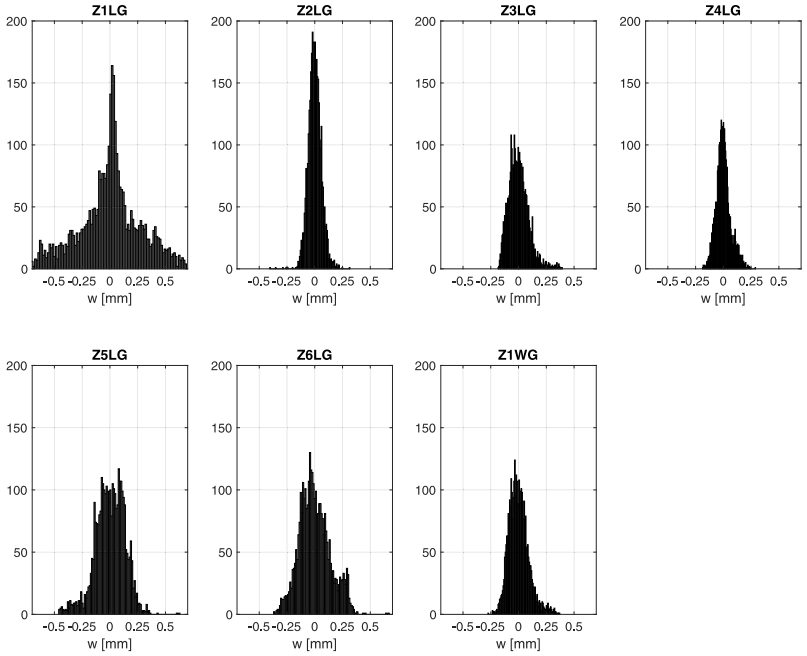

Fig. 5. Histograms of the geometric imperfections of analysed cylinders.

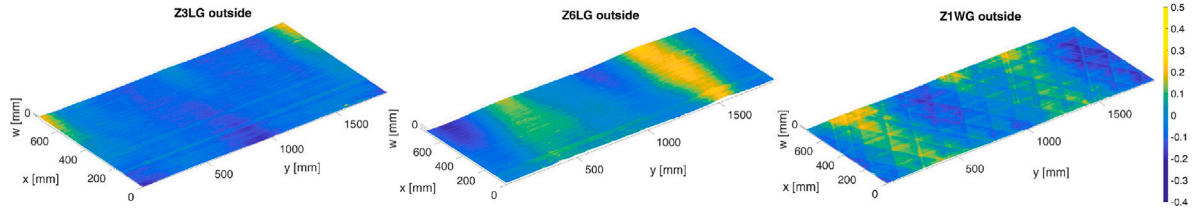

Fig. 6. Winding up pattern of Z1LG, Z6LG and Z1WG.

of the 30° layers are clearly evident in the winding-up pattern of this shell. The regular imperfection pattern is also recognisable in the Fourier coefficients. In the right-hand section of Fig. 7, the largest amplitudes of the Fourier coefficients are dominated by the 30° layers and their crossing sections. Furthermore, there are also very distinct eleventh circumferential modes, cf. the left part of Fig. 7. For shells Z1LG - Z6LG, the patterns of amplitudes of circumferential modes are similar to the filament-wound one, however, there are no distinct circumferential modes like for Z1WG.

3.2. Experimental results

Each shell was tested a minimum of 12 times across the different test rigs under axial compression until buckling, as illustrated in Fig. 8. While there are significant differences in buckling load between shells and between test rigs, it is apparent that for each configuration the buckling loads are approximately constant over the course of the experiments. Although no NDI assessment such as ultrasonic inspection is conducted, this leads to assume that no degradation by way of delamination or cracking was triggered. For each configuration, the first buckling load as well as recorded loading imperfections, if any, are given in Table 4.

Comparing the data from optical sensors and internal displacement measurement system of the Hexapod yields an average axial stiffness of 101.5 ± 2.9 kN/mm across all shells. Variation of stiffnesses between Z1LG with the lowest value of 97.0 kN/mm and Z1WG with the highest recorded stiffness at 104.5 kN/mm can likely be attributed to varying wall thicknesses between shells. Indeed, taking the load carrying wall thickness into account results in a smeared axial Young's modulus of 53.1 ± 0.9 GPa considering all shells. In contrast, data from external displacement transducers in experiments at the DLR buckling facility yield axial stiffness values about 7% lower than those recorded at the Hexapod. This difference may well be founded in the attachment of the sensors on the two test rigs. While the optical sensors in the Hexapod setup measure strictly the change of distance between the shell clampings, the transducers in the DLR setup may also record the inplane deformation of the shells in those clampings and of the epoxy concrete layers used for optimal alignment.

The shell Z6LG reaches the highest buckling load in all tested configurations. A buckling load of 59.09 kN is recorded on the Hexapod, while a buckling load of 77.95 kN is achieved in the DLR buckling

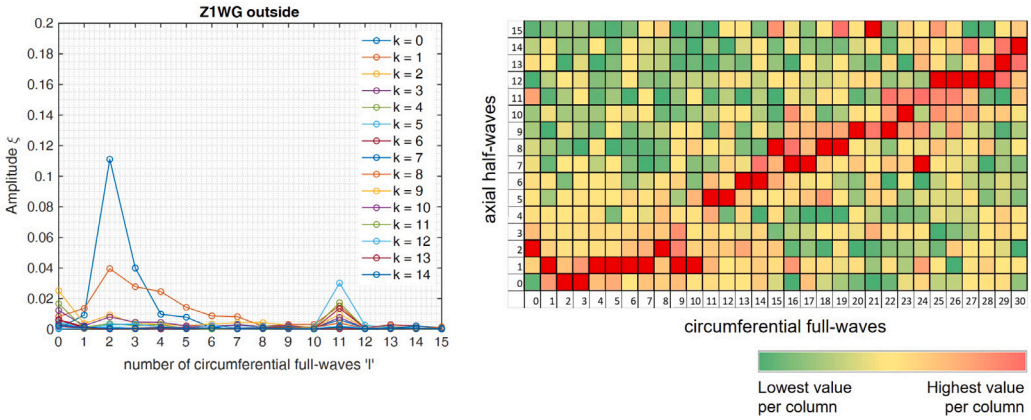

Fig. 7. Fourier coefficients of Z1WG.

Table 4
Buckling loads of the cylinders.

	Z1LG	Z2LG	Z3LG	Z4LG	Z5LG	Z6LG	Z1WG
Buckling load Hexapod [kN]	52.27	52.40	53.1	57.63	55.92	59.09	60.30
Lateral force [kN]	0.31	0.28	0.37	0.14	0.5	0.58	0.16
Lateral force direction	−111.47°	−44.1°	−52.3°	108.3°	−136.4°	−53.4°	−180.8°
Tilting angle	0.002°	0.006°	0.004°	0.003°	0.004°	0.002°	0.003°
Tilting direction	7.9°	44.1°	26.2°	78.0°	44.7°	57.4°	87.4°
Torsional moment [kN m]	0.47	0.45	0.30	0.43	0.36	0.38	0.53
Buckling load DLR [kN]	–	–	–	–	65.70	77.95	–

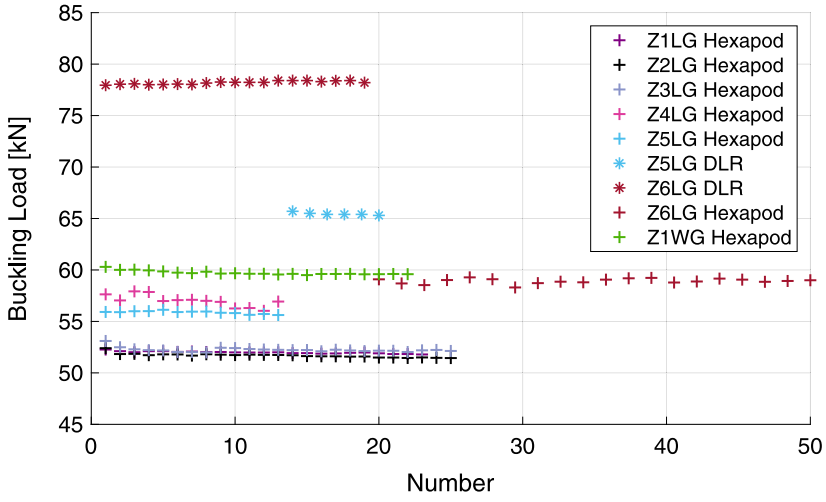

Fig. 8. Buckling loads of the tested cylinders.

facility. Shell Z5LG is tested on the Hexapod with a buckling load of 55.92 kN, while the DLR buckling facility achieves a buckling load of 65.70 kN. This means that the buckling load in the DLR buckling facility is 17.5% or 31.9% higher than in the Hexapod. During all tests on the Hexapod, recorded lateral forces are comparatively low, amounting to less than 1% of the axial buckling load for all shells. These reaction forces at the lower clamping may arise for example from imperfect alignment between shell and test rig or local variation of stiffness along the circumference of a shell. The tilt introduced during testing is between 0.002° and 0.006° in the Hexapod setup. This does not include possible tilting present before the start of a test due to tolerances of the test setup. However, the direction of the recorded tilt is always in the first quadrant. Furthermore, a resulting torsional moment of 0.30 kNm to 0.53 kNm is measured for all shells.

In Fig. 9, two representative load displacement curves of Z6LG are plotted. One was recorded on the Hexapod test rig and one in the DLR buckling facility. As displacement on the Hexapod is recorded directly at the shell, the stiffness is with 103.65 kN/mm higher than the one recorded at the DLR buckling facility. Here, the displacement of the epoxy concrete layers and the clamped parts of the shell is also measured and leads to a stiffness of 96.45 kN/mm. In addition to the smaller buckling load on the Hexapod, the area before buckling is particularly interesting. A flattening of the force displacement curve occurs here, which indicates localised pre-buckling. This was also audible during the test. In tests on the DLR buckling system, this did not occur with either Z5LG or Z6LG. Fig. 10 depicts the post-buckling pattern of Z6LG, which was recorded using a DIC measurement carried out with an ARAMIS system.

3.3. Numerical analysis

Applying all of the real, measured imperfection patterns to a set of identical shells of nominal geometry, as described in Section 2.3, results

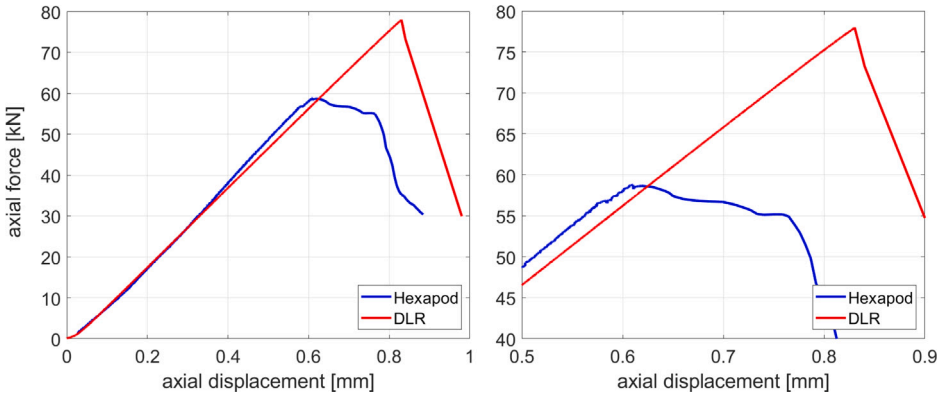

Fig. 9. Load displacement curve of Z6LG.

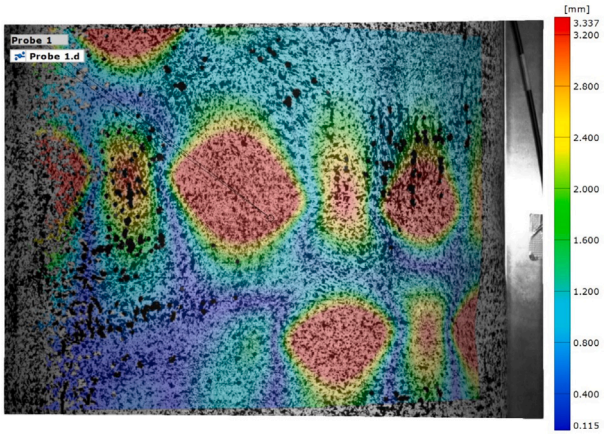

Fig. 10. Section of buckling pattern of Z6LG measured by DIC.

in significant variation of buckling loads. In Fig. 11 the influence on the buckling load is depicted. The perfect buckling load of a shell in this setup is 78.74 kN. The imperfection pattern of shell Z5LG shows the largest reduction in buckling load at 23.0%. The imperfection patterns of the shells Z2LG, Z3LG and Z4LG reduce the buckling load between 18.8% and 20.8%. In contrast, the imperfection patterns of Z1LG, Z6LG and Z1WG decrease buckling loads in the given setup only by about 10.0%.

In the following, the results of the second numerical study described in Section 2.3 are presented. For this study the advanced model is utilised. The influence factors on the buckling load of each shell are plotted in Fig. 12. Due to the manufacturing process different lay-ups occur in the filament wound shell Z1WG. Therefore, a symmetrical and balanced layup are implemented for this shell. Considering geometric imperfections reduces the buckling load between 6 kN and 19 kN. As shown in the first numerical study, the imperfection pattern of Z5LG causes the largest reduction. Taking load imperfections by way of lateral force in addition to the geometric imperfections into account, the numerical buckling load changes on average by 0.20 kN. For Z6LG the buckling load decreases by 0.70 kN, whereas for Z5LG it slightly increases by approximately 0.20 kN. Including measured torsional moments reduces the buckling load by up to 0.40 kN. As has also been shown in previous studies, e.g. [39], due to direction dependent interactions between geometric and loading imperfections in some cases imperfect load introduction may cause an increase in buckling loads. Some further interaction may occur between the different imperfection types, as considering the sum of load reductions from each influence separately versus a simulation considering all factors simultaneously yields different results in some cases. The mean reduction of buckling load caused by geometric imperfections is 12.55 kN, while lateral loads, torsional moments and tilting yield on average reduction by 0.05 kN, 0.15 kN and 7.43 kN respectively. For Z1WG with a balanced layup as well as Z3LG the largest discrepancy between addition of the individual influences and the simulation including all influences are found, amounting to 0.81 kN and 0.61 kN respectively. The average discrepancy over all shells is 0.42 kN.

Table 5
Simulated shell tilting.

	Z1LG	Z2LG	Z3LG	Z4LG	Z5LG	Z6LG	Z1WG
Tilting angle at buckling	0.024°	0.020°	0.023°	0.010°	0.006°	0.021°	0.024°
Tilting direction	160°	−115°	120°	10°	−120°	−65°	100°

Despite including all measured imperfections and considering the boundary conditions of the shells, in many cases it is not possible to numerically achieve buckling loads within 5% of the experimental results conducted on the Hexapod. Thus, it stands to reason that other influencing factors need to be considered, which have not been measured. The influence of numerous non-quantifiable factors originating from test rig and test setup are approximated in simulations by introducing an equivalent inclination that is applied to the upper shell edge.

Possible unquantified factors include:

- Eccentricity of load introduction with respect to the test rig.
- Inclination of the cylinder axis with respect to the test rig based on tolerances of the clamping, adapter plates and tolerances of the test rig itself.
- Tilting or inhomogeneous strain at the upper shell edge applied during mounting within the test rig.

The upper limit of the equivalent inclination angle is set to 0.024° which corresponds to a deviation of 0.025 mm over the diameter of a shell. This value was estimated based on occurring tolerances of the test set-up. During this study the inclination angle was increased stepwise up to the given values in Table 5. The direction of the tilting angle was chosen in each case so that the direction of reaction moments at the bottom of the shell is in accordance with the experimental one. As with lateral forces, variation of the circumferential tilting direction resulted in changes of buckling load due to interaction with the geometric imperfections of the shells. The exemplary visualisation in Fig. 13 for shell Z1LG shows changes in buckling load of 1.8 kN even for a small tilt of 0.004° depending on the circumferential tilting direction. Amplitudes of the inclination angle are chosen to achieve a good fit with the experimental buckling loads, however, no higher value than the given limit is permitted.

In case of Z2LG and Z4LG to Z6LG good approximation of the buckling load is reached. Taking at least one type of imperfection into account the buckling load of Z1WG is smaller if a balanced lay-up is assumed, whereas for the perfect buckling load a higher value is reached if a balanced lay-up is assumed instead of a symmetric one.

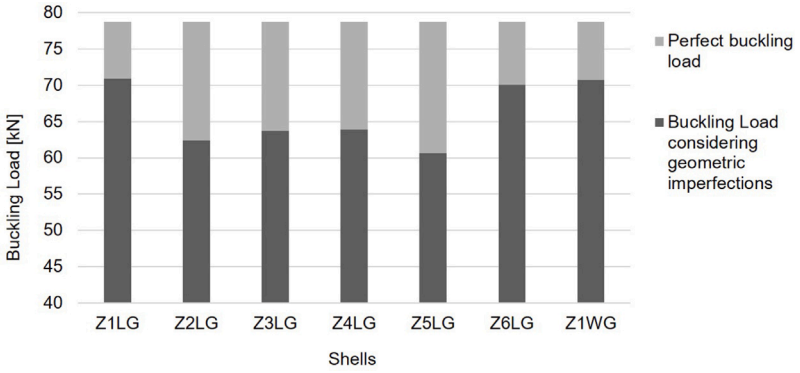

Fig. 11. Influence of the different imperfection patterns.

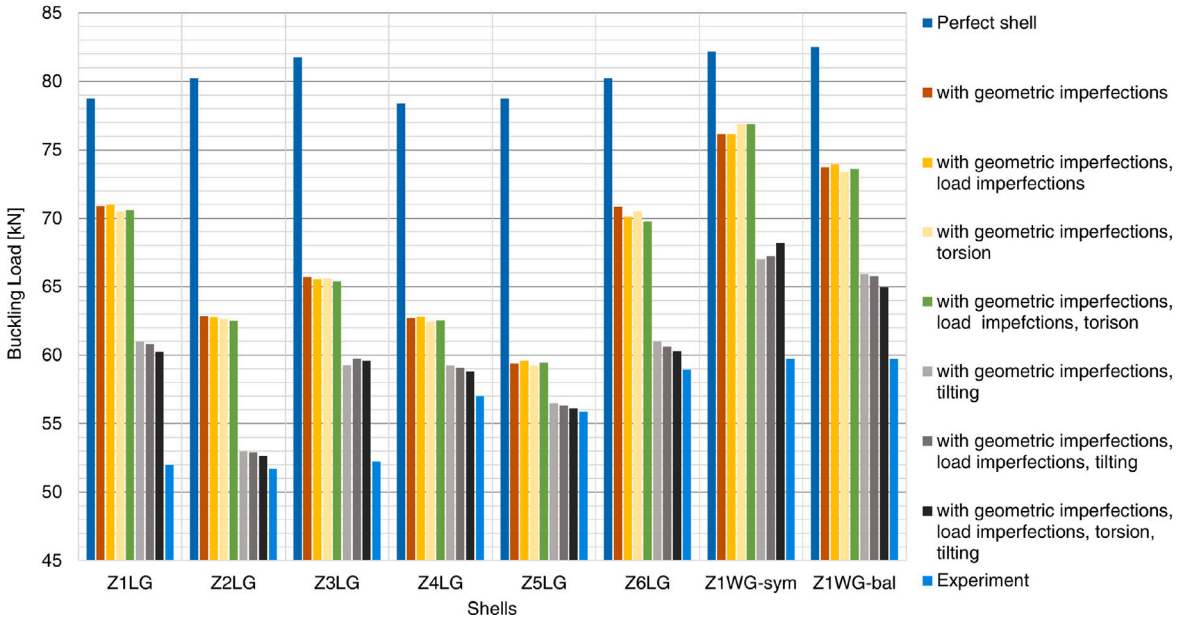

Fig. 12. Comparison of the different influencing factors on the buckling load.

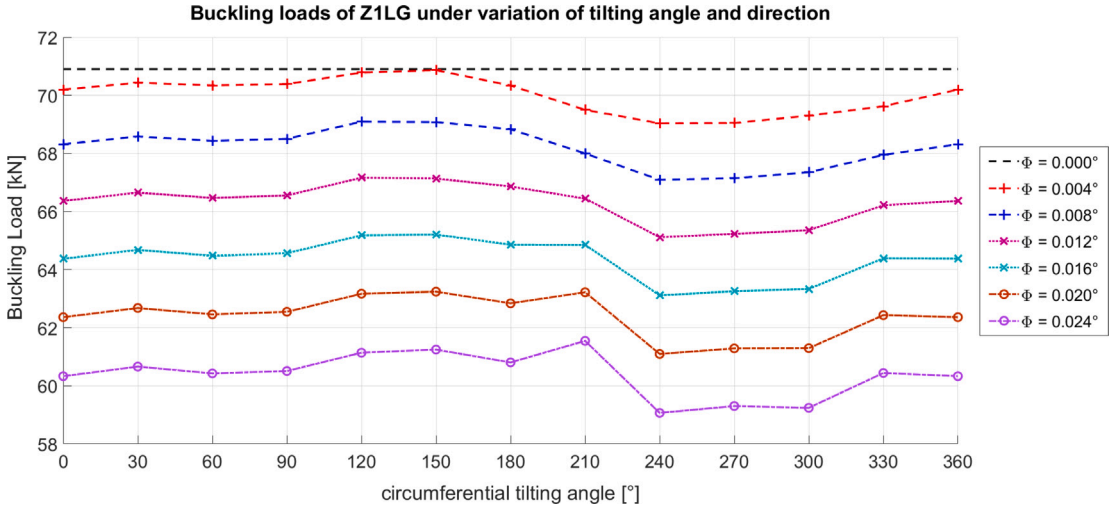

Fig. 13. Numerical buckling loads resulting from circumferential variation of tilting angle.

In the next step, the quality of three different utilised models described in Section 2.3 is analysed. Furthermore, model validation is performed for these models. According to recommendations of NASA SP-8007 this is done based on the stiffness of the shell [4]. In Table 6 beside the numerical and perfect buckling loads of each shell in each model configuration, the numerical stiffness is given. For shells Z1LG -

Table 6
Buckling loads and stiffnesses determined from simulations.

	Z1LG	Z2LG	Z3LG	Z4LG	Z5LG	Z6LG	Z1WG
Buckling loads [kN]							
Free length model	62.46	52.69	60.27	59.81	57.18	62.11	65.76
Full length model	62.26	53.26	60.64	59.80	57.09	60.94	62.64
Advanced model	62.42	52.90	60.32	59.60	57.15	60.49	61.46
Shell stiffnesses [kN/mm]							
Free length model	102.59	102.54	103.16	102.78	102.24	102.83	103.46
Full length model	96.12	96.10	96.59	96.29	95.76	96.11	96.92
Advanced model	99.03	99.03	99.54	99.22	98.70	99.10	99.00
Perfect buckling loads [kN]							
Free length model	78.79	80.30	81.81	78.47	78.79	80.30	82.10
Full length model	78.78	80.28	81.79	78.45	78.78	80.28	82.09
Advanced model	79.03	80.54	82.06	78.70	79.03	80.54	82.82

Z6LG the free length model overestimates the stiffness by 2.10%. The full length model and the advanced model underestimate the stiffness by 4.55% and 1.44% respectively. According to NASA SP-8007 the requirement for a high fidelity model is a stiffness deviation of less than 2% [4]. This requirement is fulfilled by the advanced model. In contrast, the advanced model of the filament wound shell underestimates the stiffness by 5.5%. The buckling load for shell Z1LG - Z6LG is on average 2.7% and 1.9% higher if the free length or full length model is utilised instead of the advanced model, whereas the perfect buckling load of these shells is on average 1,8% or 1.9% lower if these models are used. In contrast, for Z1WG the free length model gives a 7.0% higher buckling load than the advanced one. Using the full length model results in a 1.90% higher buckling load. The perfect buckling load of Z1WG is for both simplified models 0.9% lower than that of the advanced model.

Finally, design loads of different design approaches are presented in Table 7. For the deterministic approaches, nominal parameters are chosen. With exception of the PPLA, the probabilistic approaches use the given parameters. Since Fourier coefficients are only available for the free length, for FMC and the SAP only free length is considered.

The lowest design load is given by NASA SP-8007 and the LBMI with an imperfection amplitude equal to the average shell wall thickness. The highest design load is provided by the SPLA. This design load is higher than almost all experimental results. The LBMI with an imperfection amplitude of a tenth of the wall thickness, the SBPA and FMC deliver design loads between 52.2 kN and 56.2kN. The SAP yields significantly smaller design loads than the FMC due to the much larger resulting standard deviation. Carrying out the SAP without consideration of load imperfections results in an even broader buckling load distribution of 62.13 ± 9.89 kN. As shown in [14], the Taylor series approach utilised may result in large errors if the step size for calculation of derivatives is too large. Hence, the SAP is also carried out with the same data but with step size Δz reduced from the default value of 1.5 to 1.0 and 0.5, yielding a buckling load distribution of 57.70 ± 12.86 kN and 51.3 ± 17.50 kN, respectively. On the other hand, the SAP is also applied with a lower number of Fourier coefficients while using the default step size of 1.5, as the entire random field of geometric imperfections is mapped onto only five variables by way of mahalanobis transformation and thus may be very sensitive to even small changes of one parameter. Reducing the number of coefficients from 4641 (51 axial and 91 circumferential) to 1073 results in a buckling load distribution of 72.32 ± 5.32 kN and further reduction to 285 coefficients yields 79.18 ± 2.58 kN.

4. Discussion

In this section the results are discussed and compared with those of a study in [25] where twelve cylindrical shells with the same lay-up but significantly smaller radius are tested on the same test rigs. The manufacturing process has an influence on the imperfection pattern as shown in Section 3.1. The imperfection pattern of the filament wound shell is more regular. This also holds true for the small shells in [25,40]. The imperfection range compared to the laid shells is relatively small, leading to a smaller influence on the buckling load, as shown in the first study in Section 3.3. Similar behaviour was also shown in the study with the smaller shells in [25]. However, the sample size of one large wound shell is rather small for further conclusions. In general, the shells in this paper show a significantly higher imperfection sensitivity due to their R/t-ratio, which is also apparent in the influence of geometric imperfections. While geometric imperfections reduce the buckling load on average between 1% and 5% for the small shells in [25], it is 7.3% up to 24.1% for the larger shells in this contribution.

Furthermore, the test rig has a significant influence on the buckling load. As shown in Section 3.2, in the DLR buckling facility higher buckling loads are achieved. The difference is between 17.5% and 31.5% in comparison to the Hexapod. For the thicker, smaller shells in [25] the difference among these two test rigs is between 0.2% and 5.4%. The significantly higher imperfection sensitivity for thinner large shells is also evident here. In [25] it was shown that the difference is mainly due to the epoxy compensation layer which enables a very even load distribution on the shells. Consequently, a buckling load close to the perfect buckling load can even be achieved for Z6LG in the DLR buckling facility. The experimental buckling load is indeed higher than the numerical one if only geometric imperfections are considered. However, this quality of load distribution is not given for the Hexapod test set-up. In fact, including geometric imperfections and the perturbations introduced during the test is not sufficient to simulate the experimental buckling load. A further misalignment has to be assumed due to the test setup, which was already present before conducting the test. This effect can be avoided on the DLR buckling facility due to the compensation layer. Comparison of the force–displacement curves of Z6LG supports this conclusion. In tests carried out on the Hexapod, pre-buckling is caused by a non-ideal load introduction, which also induces a lower buckling load. However, this did not occur during tests on the DLR buckling facility using the compensation layers. Such effects probably also occurred on the small cylinders but are not noticeable due to their lower imperfection sensitivity. Indeed, the measured disturbance quantities and geometric imperfections are sufficient for good approximation of buckling loads.

In order to allow for assessing the quality of design approaches more accurately, two performance indicators are introduced. The first indicator is precision. It indicates how accurately the experimental buckling load is predicted on average. The second one is conservativeness. This indicator specifies how frequently the design load is conservative. In Table 8 the indicators are given for analysed design approaches from Section 3.3. Since the buckling load depends on the test rig, this is also done for each setup separately. As only one wound shell was tested, this evaluation is only based on the layered shells Z1LG to Z6LG.

Design loads provided by NASA SP-8007 are consistently very conservative, which is also indicated by the low precision. This is according to many results in literature. Applying the LBMI with imperfection scale of the wall-thickness leads to very conservative results even lower than those of NASA SP-8007. However, using an imperfection scale factor of 0.1 of the wall thickness yields more precise results. In that case, rather 50% of design loads are conservative. For comparison, the average rms-value of imperfections is about 0.13 mm. Comparing the buckling load of the high fidelity model which only takes geometric imperfections into account, shows that even the small imperfection scaling factor overestimated the influence of geometric imperfections. The precision of the SPLA is better than that of NASA SP-8007 and partly the LBMI. In case of the results determined at the DLR buckling facility a precision of about 90% is reached. But only in one case the given design load is conservative. As shown in [10], the SPLA covers primarily the effect of geometric imperfections. However, in many of the test results geometric imperfections are not the only buckling driving quantity. Furthermore, as also shown in [10] if symmetric or

Table 7
Design loads calculated by different design approaches.

Design approach	Design load	Radius	Length	Layer thickness	Buckling load distribution
NASA SP-8007	33.61 kN	300 mm	800 mm	0.133 mm	–
LBMI ($\xi = t$)	28.81 kN	300 mm	800 mm	0.133 mm	–
LBMI ($\xi = 0.1t$)	56.17 kN	300 mm	800 mm	0.133 mm	–
SPLA	68.02 kN	300 mm	800 mm	0.133 mm	–
SBPA	52.44 kN	300 mm	800 mm	0.133 mm	–
PPLA (0.99)	52.36 kN	300.2 mm	800 mm	0.134 ± 0.002 mm	60.04 ± 3.30 kN
PPLA (0.90)	55.81 kN	300.2 mm	800 mm	0.134 ± 0.002 mm	60.04 ± 3.30 kN
FMC (0.99)	52.15 kN	300.2 mm	750 mm	0.134 ± 0.002 mm	61.09 ± 3.84 kN
FMC (0.90)	56.17 kN	300.2 mm	750 mm	0.134 ± 0.002 mm	61.09 ± 3.84 kN
SAP (0.99)	38.34 kN	300.2 mm	750 mm	0.134 ± 0.002 mm	58.86 ± 8.39 kN
SAP (0.90)	47.10 kN	300.2 mm	750 mm	0.134 ± 0.002 mm	58.86 ± 8.39 kN

Table 8
Precision and Conservativeness of the different analysed design approaches.

Design approach	Hexapod		DLR		Both	
	Precision	Conservativeness	Precision	Conservativeness	Precision	Conservativeness
NASA SP-8007	61.7%	100%	47.1%	100%	57.7%	100%
LBMI ($\xi = t$)	52.4%	100%	40.4%	100%	49.4%	100%
LBMI ($\xi = 0.1t$)	95.3%	33.3%	78.8%	100%	91.2%	50%
SPLA	76.2%	0%	91.9%	50%	80.1%	12.5%
SBPA	95.3%	66.7%	73.6%	100%	89.9%	75.0%
PPLA (0.99)	95.2%	83.3%	73.4%	100%	89.8%	87.5%
PPLA (0.90)	95.5%	50.0%	78.3%	100%	91.2%	62.5%
FMC (0.99)	94.9%	100%	73.1%	100%	89.5%	100%
FMC (0.90)	95.3%	33.3%	78.8%	100%	91.2%	50.0%

balanced lay-up is used, it is not possible to predict with certainty whether the SPLA provides conservative or non-conservative results. In contrast, the SBPA delivers on average more precise design loads then SPLA. Here, results are in most cases conservative. Since the SBPA takes imperfect boundary conditions into account, a good precision of buckling prediction of the Hexapod test results is given.

Compared to the experimental buckling load of 55.07 ± 2.91 kN on the Hexapod, the FMC overestimates mean value and standard deviation. The SAP exhibits high sensitivity to variation of the finite difference step. Based on the results presented in Section 3.3, it stands to reason that in addition to the possibility of choosing unfavourable points to evaluate the objective function which leads to an unrepresentative distribution as shown in [39], the individual manufacturing of the shells and the available sample size lead to the generation of unrealistic imperfection patterns for this approach. Consequently, decreasing the number of Fourier coefficients does reduce the volatile scatter in buckling load, but at the cost of precision and conservativeness, as it is shown in a parameter study that numerical buckling loads start to increase significantly when using less than about 4600 coefficients.

In summary, since precision and conservativeness differ for the approaches between the results determined on different test rigs, the over all trend which approaches are suitable for these shells is consistent. Therefore, when choosing a design approach, it should be considered which influencing factors are taken into account. Since non-uniformities in load introduction have a strong influence on the buckling load, at least in tests on the Hexapod, approaches that take this into account provide good approximation of the buckling load. This is the case for the SBPA or the FMC, for instance. The NASA SP-8007 covers everything with its strong conservatism. In contrast, the SPLA does not provide reliable design loads, similar to the LBMI. However, in literature the question is raised how realistic Eigenmodes are as geometric imperfections. The SAP, meanwhile, is not suitable for the design of the given cylindrical shells, since no representative imperfection patterns are generated at the evaluation points of the algorithm.

5. Conclusion

In this paper, seven cylindrical shells were tested and influencing factors on the buckling load were determined. Tests were carried out on two different test rigs and the shells were manufactured in two different processes. The investigated shells are compared with similar but significantly thicker and smaller shells from an earlier study. Generally, the shells show a significant sensitivity to disturbing factors on the buckling load. This applies to geometric imperfections, but especially to load imperfections and tilting introduced during testing. While the manufacturing process has a comparatively small influence on the buckling load, the test rigs have a major influence on the buckling load. This is quantified in this publication. It is demonstrated which influences must be taken into account when evaluating test data in order to ensure that subsequent design developments and validation are meaningful. Therefore, the quality should always be quantified when publishing test data. This can be done using test rig comparisons or validated FE models, as both are shown in this publication. If this is not done, other researchers may draw wrong conclusions when using the provided data. In application of different design approaches, it becomes apparent that some approaches do not cover all influencing factors. If such factors are expected, an approach should be selected that also takes these into account. A list of the influencing factors considered might be helpful here. In principle, it is recommended to conduct further test rig comparisons for better assessment of test data and a critical analysis of existing test data.

CRediT authorship contribution statement

Tobias S. Hartwich: Writing – original draft, Visualization, Methodology, Investigation, Conceptualization. **Stefan Panek:** Writing – original draft, Visualization, Investigation, Formal analysis. **Dirk Wilckens:** Writing – original draft, Investigation. **Tobias Wille:** Resources. **Dieter Krause:** Writing – review & editing, Supervision, Project administration, Funding acquisition.

Declaration of competing interest

The authors declare that they have no known competing financial interests or personal relationships that could have appeared to influence the work reported in this paper.

Data availability

Data will be made available on request.

Acknowledgements

This research was funded by German Research Foundation (DFG) via the project *Zuverlässigkeitsbasierte Auslegung unversteifter CFK-Zylinderschalen unter Material- und Strukturunsicherheiten*. The Hexapod was also funded by the DFG. Finally, we would like to acknowledge Dirk Röstermundt, who passed away too soon, for manufacturing the cylinders and his valuable contribution to the success of the project mentioned above.

References

[1] Degenhardt R, Castro SG, Arbelo MA, Zimmerman R, Khakimova R, Kling A. Future structural stability design for composite space and airframe structures. Thin-Walled Struct 2014;81:29–38.
[2] Rudd MT, Schultz MR, Gardner NW, Kosztowny CJ, Bisagni C. Testing of a composite conical-cylindrical shell. In: AIAA SCITECH 2023 forum. Reston, Virginia: American Institute of Aeronautics and Astronautics; 2023.
[3] Singer J, Arbocz J, Weller T. Buckling experiments: Experimental methods in buckling of thin-walled structures. Chichester: Wiley; 2002.
[4] Hilburger MW. NASA-SP-8007-2020/REV 2: Buckling of thin-walled circular cylinders. 2020.
[5] Koiter WT. A translation of the stability of elastic equilibrium. Air Force Flight Dynamics Laboratory; 1970.
[6] Degenhardt R, Kling A, Bethge A, Orf J, Kärger L, Zimmermann R, Rohwer K, Calvi A. Investigations on imperfection sensitivity and deduction of improved knock-down factors for unstiffened CFRP cylindrical shells. Compos Struct 2010;92(8):1939–46.
[7] Schillo C, Röstermundt D, Krause D. Experimental and numerical study on the influence of imperfections on the buckling load of unstiffened CFRP shells. Compos Struct 2015;131:128–38.
[8] Hühne C, Rolfes R, Breitbach E, Teß mer J. Robust design of composite cylindrical shells under axial compression — Simulation and validation. Thin-Walled Struct 2008;46(7–9):947–62.
[9] Kalnins K, Arbelo MA, Ozolins O, Castro SG, Degenhardt R. Numerical characterization of the knock-down factor on instiffened cylindircal shells with initial geometric imperfections. In: 20th international conference on composite 2015. 2015.
[10] Kriegesmann B, Jansen EL, Rolfes R. Design of cylindrical shells using the single perturbation load approach – potentials and application limits. Thin-Walled Struct 2016;108:369–80.
[11] Schillo C, Kriegesmann B, Krause D. Reliability based calibration of safety factors for unstiffened cylindrical composite shells. Compos Struct 2017;168:798–812.
[12] Khakimova R, Castro SG, Wilckens D, Rohwer K, Degenhardt R. Buckling of axially compressed CFRP cylinders with and without additional lateral load: Experimental and numerical investigation. Thin-Walled Struct 2017;119:178–89.
[13] Arbocz J, Hilburger MW. Toward a probabilistic preliminary design criterion for buckling critical composite shells. AIAA J 2005;43(8):1823–7.
[14] Kriegesmann B, Rolfes R, Hühne C, Kling A. Fast probabilistic design procedure for axially compressed composite cylinders. Compos Struct 2011;93:3140–9.
[15] Meurer A, Kriegesmann B, Dannert M, Rolfes R. Probabilistic perturbation load approach for designing axially compressed cylindrical shells. Thin-Walled Struct 2016;107:648–56.
[16] Takano A. Statistical knockdown factors of buckling anisotropic cylinders under axial compression. J Appl Mech 2012;79(5).
[17] Wagner H, Hühne C, Elishakoff I. Probabilistic and deterministic lower-bound design benchmarks for cylindrical shells under axial compression. Thin-Walled Struct 2020;146:106451.
[18] Wang B, Hao P, Ma X, Tian K. Knockdown factor of buckling load for axially compressed cylindrical shells: state of the art and new perspectives. Acta Mech Sin 2022;38(1).
[19] Hartwich TS, Panek S. Database of static buckling experiments with cylindrical composite shells under axial compression. 2023.
[20] Panek S, Hartwich TS, Kriegesmann B, Krause D. Guidelines for test conditions and documentation of buckling experiments with cylindrical CFRP shells. In: 23rd international conference on composite materials. ICCM23, 2023.
[21] Uemura M, Kasuya H. Coupling effect on axial compressive buckling of laminated composite cylindrical shells. In: ICCM-IV. 1982.
[22] Bisagni C. Experimental buckling of thin composite cylinders in compression. AIAA J 1999;37(2):276–8.
[23] Takano A. Buckling experiment on anisotropic long and short cylinders. Adv Technol Innov 2016;1(1).
[24] Tasi J, Feldman A, Stang DA. NASA CR-266 - the buckling strength of filament-wound cylinders under axial compression. 1965.
[25] Hartwich TS, Panek S, Wilckens D, Bock M, Krause D. The influence of the manufacturing process and test boundary conditions on the buckling load of thin-walled cylindrical CFRP shells. Compos Struct 2023;308:116674.
[26] Meyer-Piening H-R, Farshad M, Geier B, Zimmermann R. Buckling loads of CFRP composite cylinders under combined axial and torsion loading – experiments and computations. Compos Struct 2001;53(4):427–35.
[27] Bisagni C. Composite cylindrical shells under static and dynamic axial loading: An experimental campaign. Prog Aerosp Sci 2015;78:107–15.
[28] Franzoni F, Odermann F, Lanbans E, Bisagni C, Andrés Arbelo M, Degenhardt R. Experimental validation of the vibration correlation technique robustness to predict buckling of unstiffened composite cylindrical shells. Compos Struct 2019;224:111107.
[29] Hipp P, Jensen D. Design and analysis of filament-wound cylinders in compression. In: 33rd structures, structural dynamics and materials conference. Reston, Virigina: American Institute of Aeronautics and Astronautics; 1992, p. 2442–52.
[30] Wagner H, Hühne C, Niemann S. Robust knockdown factors for the design of axially loaded cylindrical and conical composite shells – development and validation. Compos Struct 2017;173:281–303.
[31] Plaumann B, Rasmussen O, Krause D. System analysis and synthesis for the dimensioning of variant lightweight cabin interior. In: 54th AIAA/ASME/ASCE/AHS/ASC structures, structural dynamics, and materials conference. 2013.
[32] Hartwich TS, Krause D. The influence of geometric imperfections of different tolerance levels on the buckling load of unstiffened CFRP cylindirical shells. In: 22th international conference on composite materials. ICCM22, 2019, p. 4502–11.
[33] Xin R, Le VT, Goo NS. Buckling identification in composite cylindrical shells with measured imperfections using a Multi-DIC method and finite element analysis. Thin-Walled Struct 2022;177:109436.
[34] Rudd MT, Eberlein DJ, Waters WA, Gardner NW, Schultz MR, Bisagni C. Analysis and validation of a scaled, launch-vehicle-like composite cylinder under axial compression. Compos Struct 2023;304:116393.
[35] Hartwich TS, Völkl H, Wartzack S, Krause D. Designing lightweight structures under consideration of material and structure uncertainties on different levels of the building block approach. In: Proceedings of the 31st symposium design for X. DFX2020, The Design Society; 2020, p. 121–30.
[36] Taheri-Behrooz F, Omidi M. Buckling of axially compressed composite cylinders with geometric imperfections. Steel Compos Struct 2018;29(4):557–67.
[37] Castro SGP, Zimmermann R, Arbelo MA, Khakimova R, Hilburger MW, Degenhardt R. Geometric imperfections and lower-bound methods used to calculate knock-down factors for axially compressed composite cylindrical shells. Thin-Walled Struct 2014;74:118–32.
[38] Hartwich TS, Panek S, Krause D. Geometric imperfection data of 7 thin-walled cylindrical shells with R/t-ratio of 375. 2024.
[39] Panek S, Hartwich TS, Krause D. Directional effects of load deviations on the buckling of cylindrical shells in experiment and design. In: Proceedings of the 33rd symposium design for X. DFX2022, 2022.
[40] Hartwich TS, Panek S, Krause D. Geometric imperfection data of 12 thin-walled cylindrical shells with R/t-ratio of 147. 2024.